

Reaction scheme and kinetic modelling for the MTO process over a SAPO-18 catalyst

A.G. Gayubo*, A.T. Aguayo, A. Alonso, A. Atutxa, J. Bilbao

Departamento de Ingeniería Química, Universidad del País Vasco, Apartado 644, 48080 Bilbao, Spain

Available online 22 August 2005

Abstract

A kinetic model for simulation of the MTO process over SAPO-18 catalyst in a wide range of operating conditions has been proposed. The kinetic model predicts the experimental evolution of reaction products with time on stream, which follows three consecutive periods: initiation (where olefin production increases), a period of maximum olefin production and a period in which this production decreases. The kinetic scheme takes into account these three steps that evolve with time on stream: formation of active intermediate compounds, an step where olefins are formed by reaction of oxygenates (methanol/DME) with these intermediates and deactivation of intermediates by degradation to coke. The presence of water in the reaction medium attenuates the reaction rate of these steps. Discrimination of kinetic equations and calculation of the parameters of best fit have been carried out by solving the mass conservation equations of the individual components of the kinetic scheme together with the kinetic equation for deactivation and taking into account the effect of water on the kinetics of each step. © 2005 Elsevier B.V. All rights reserved.

Keywords: SAPO-18; MTO process; Kinetic modelling; Deactivation; Carbon pool mechanism

1. Introduction

The interest of the MTO process (transformation of methanol into olefins) is a consequence, on the one hand, of the increasing demand for olefins, and on the other, serves to boost the valorization of alternative raw materials to oil (coal, natural gas, biomass), which may be transformed into methanol via syngas [1]. The industrial implementation of the MTO process has been possible thanks to the high activity and selectivity to olefins of the SAPO-34 catalyst. Although the technological development of this process has been considerable, kinetic modelling has yet to be fully developed. This gap is common to most catalytic processes, although kinetic modelling is vital for simulation of processes that, as in the case of MTO, are carried out at large-scale and are important from an economic perspective. The explanation of this gap lies in the difficulty for studying the kinetics when the process follows complex reaction schemes, and the difficulty is compounded when

catalyst deactivation is very rapid, as happens in the MTO process.

Two types of kinetic models have been proposed in the literature for the MTO process on SAPO-34: (a) detailed models, that consider the individual reaction of each component [2–4] and (b) simplified models made up of “lumps” or groups of components with similar kinetic behaviour. In these models, the mechanistic aspects are considered in a generic way and, as they are simpler, they have advantages both for obtaining kinetic parameters and for their use in reactor design [5–7].

The few quantitative studies in the literature on the deactivation kinetics of the MTO process correspond to SAPO-34 catalyst. Bos et al. [6] quantify the deactivation by means of empirical equations that relate the kinetic constants to the coke content in the catalyst. Alwahabi and Froment [4] propose similar equations by attributing coke nature to C₆–C₈ olefins formed by oligomerization of light olefins, which are trapped in the catalyst cages due to the severe shape selectivity of SAPO-34 (with 3.8 Å size pores). Gayubo et al [8] have proposed kinetic models by taking into account the effect of water as attenuating agent of coke deposition.

* Corresponding author. Tel.: +34 94 601 5449; fax: +34 94 601 3500.
E-mail address: iqpgacaa@lg.ehu.es (A.G. Gayubo).

Nomenclature

A, O, R, W	oxygenates (methanol + DME), olefins, intermediate compound and water
a	activity of the catalyst defined as ratio of reaction rates (Eq. (8))
k_i, k_d	kinetic constants for each step of the kinetic scheme (Fig. 1) and for deactivation (h^{-1})
r_i, r_d	reaction rate for the formation of each i component of the kinetic scheme and for deactivation
W/F_o	space-time ($\text{g catalyst h (g MeOH)}^{-1}$)
t	time on stream (h)
X_i, X_{w_o}	mass fraction of each i component in the reaction medium, and of water in the feed, by mass unit of CH_2 units ($\text{g (g CH}_2\text{)}^{-1}$)
Y_R	mass fraction of the intermediate compounds by mass unit of fresh catalyst ($\text{g (g catalyst)}^{-1}$)
<i>Greek symbols</i>	
α	standardised amount of intermediate compound trapped in the cages of SAPO-18
θ, θ_d	functions for attenuation by water, for the main reaction and for deactivation

This attenuation is explained by coke precursor competition in the adsorption on the acid sites.

In this paper, the kinetic modelling of the MTO process is studied on a SAPO-18 catalyst, which is an interesting alternative to SAPO-34, given that it has the following advantages: coke deactivation is significantly slower, its preparation method is simpler and the organic template is cheaper [9,10]. As in the case of SAPO-34, methanol must be fed with water in order to attenuate coke deposition. Three consecutive periods are observed in the evolution of olefin production with time on stream on SAPO-18 (especially under conditions of low reaction rate): (1) initiation, in which the main product is DME and olefin production increases, (2) maximum production of olefins and (3) deactivation. The initiation period and its dependence on process conditions are evidence of “carbon pool mechanism” [11] in the MTO process and the need for reactive intermediates (methylarene type) for olefin production [12]. The quantification of light olefin evolution with time on stream requires considering the simultaneous evolution of these three periods and their dependence on reaction conditions.

2. Experimental

The catalyst consists of 25 wt% of active phase (SAPO-18 synthesised following the method of Chen et al. [9]), agglomerated by wet extrusion with bentonite as binder

(45 wt%) and with inert alumina as charge (30 wt%), in order to confer a high mechanical resistance to attrition upon the catalyst. The physical properties of the catalyst determined by N_2 adsorption–desorption and Hg porosimetry are: BET surface area, $171 \text{ m}^2 \text{ g}^{-1}$; macropore volume, $0.15 \text{ cm}^3 \text{ g}^{-1}$; mesopore volume, $0.24 \text{ cm}^3 \text{ g}^{-1}$; micropore volume, $0.13 \text{ cm}^3 \text{ g}^{-1}$. The pore volume distribution is: $d_p < 20 \text{ \AA}$, 25%; $20 \text{ \AA} < d_p < 500 \text{ \AA}$, 46%; $500 \text{ \AA} < d_p$, 29%. From the thermogravimetric measurement of NH_3 adsorption, a total acidity of $0.12 \text{ (mmol of NH}_3\text{) (g of catalyst)}^{-1}$ has been determined at 150°C . By combining thermogravimetric and calorimetric measurements, acid strength has been proven to be very uniform with a majority of sites with a value of $140\text{--}150 \text{ kJ (mol of NH}_3\text{)}^{-1}$, and with peaks in the TPD of NH_3 at 243°C (weak acidity) and at 331°C (strong acidity). Consequently, the sites are moderately acid and have a lower density distribution than in SAPO-34 [10].

The kinetic study has been carried out in a reaction equipment provided with a fluidized bed reactor. The reactor is a vertical cylinder of S-316 stainless steel of 20 mm internal diameter and a total length of 465 mm, which is located within a ceramic chamber heated by an electric resistance. It is provided with a porous plate for supporting the catalyst bed, which is placed at 285 mm from the bottom. The operating variables are controlled by means of Adkir process control software, which has been specifically designed for this process. The catalytic bed consists of a mixture of the catalyst with a particle size between 150 and $250 \mu\text{m}$ and inert alumina with a particle size between 60 and $90 \mu\text{m}$, with a catalyst/inert ratio of 20/80 in weight. In this way, the hydrodynamic properties of the bed are improved. The reaction products leave the reactor through the upper part by passing through two filters in series in order to avoid the passage of fine catalyst particles into the line of gases. The on-line analysis of the reaction products is carried out by means of a Varian Star 3400 CX gas chromatograph provided with a flame ionization detector (FID). A capillary column (PONA Cross-linked Methyl Silicone, $50 \text{ m} \times 0.2 \text{ mm} \times 0.5 \mu\text{m}$) has been used.

3. Results

3.1. Kinetic model

The kinetic scheme (Fig. 1) takes into account three steps: (1) the dehydration of methanol to dimethyl ether (DME), (2) the formation of intermediate compounds, R (hydrocarbon pool), directly from oxygenates ($\text{A} = \text{MeOH} + \text{DME}$) or by reaction of oxygenates with the intermediates (autocatalytic step) and (3) the formation of olefins ($\text{O} = \text{C}_2\text{--C}_5$) and methane by reaction between oxygenates and intermediate compounds. In general, the concentration of olefins follows the order: propene > ethene > butenes \gg pentenes. The yield of methane is only significant above 450°C .

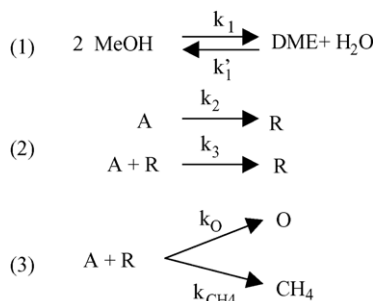


Fig. 1. Kinetic scheme for the MTO process over SAPO-18.

The kinetic equations are the following:

- Disappearance of oxygenates:

$$-r_A = \frac{dX_A}{d(W/F_o)} = -k_O X_A Y_R \theta a - k_{CH_4} X_A Y_R \theta \quad (1)$$

- Formation of olefins:

$$r_O = \frac{dX_O}{d(W/F_o)} = k_O X_A Y_R \theta a \quad (2)$$

- Formation of methane:

$$r_{CH_4} = \frac{dX_{CH_4}}{d(W/F_o)} = \frac{dX_{CH_4}}{d\tau} = k_{CH_4} X_A Y_R \theta \quad (3)$$

Eqs. (1)–(3) have been established by considering that the reactions of the kinetic scheme are elemental, and they include a function θ , Eq. (4), that quantifies the attenuating effect of water on the formation of intermediate compounds, olefins and methane [10,13]. For the θ function, an hyperbolic expression with respect to water content, X_W , has been considered, by analogy with the corresponding expression for the kinetic model of the MTO process over SAPO-34 [7].

$$\theta = \frac{1}{1 + K_W (X_W)^n} \quad (4)$$

The evolution of the intermediate product with time on stream (which has been proven to be almost independent of space-time [13]) follows the expression:

$$r_R = \frac{dY_R}{dt} = (k_2 X_A + k_3 X_A Y_R) \theta a \quad (5)$$

In Eqs. (1)–(5), the concentration of the components in the reaction medium, X_i , has been quantified as mass fraction of each component by mass unit of CH_2 units in the reaction medium (which correspond to those in the methanol feed). The concentration of active intermediates deposited on the cages of SAPO-18 is quantified as mass fraction per mass unit of fresh catalyst, Y_R .

The kinetic equation for coke deactivation, Eq. (6), includes a function, θ_d , Eq. (7), which quantifies the attenuating effect of water in the reaction medium upon coke deposition [8,14]. Activity, a , Eq. (8), is quantified as the

ratio between the olefin formation rate of the catalyst at a given time on stream (partially deactivated), r_O , and the reaction rate that the fresh catalyst would have at that time on stream under the same reaction conditions, $(r_O)_f$.

$$r_d = -\frac{da}{dt} = k_d (X_A + X_O) \theta_d a^d \quad (6)$$

$$\theta_d = \frac{1}{1 + K_{Wd} (X_W)^{n_d}} \quad (7)$$

$$a = \frac{r_O}{(r_O)_f} = \frac{[dX_O/d(W/F_o)]}{[dX_O/d(W/F_o)]_f} \quad (8)$$

This definition of activity is suitable for autocatalytic reaction systems with an initiation period in which product formation increases. On the basis of these expressions, activity gradually decreases from a value of 1 for zero time on stream, whereas product formation rate, r_O , starts at a value of zero, passes through a maximum and then decreases.

3.2. Methodology for model discrimination and calculation of kinetic parameters

Discrimination of models and calculation of kinetic parameters has been carried out by fitting the experimental values of component composition with time on stream to the mass conservation equations obtained according to the kinetic scheme, and by using the kinetic equations, Eqs. (1)–(5), for products and Eqs. (6)–(8) for deactivation. Plug flow has been assumed for the gas. The kinetic modelling of the process requires simultaneously solving the kinetic equations for the main reaction and for deactivation, given that the autocatalytic effect of the main reaction and catalyst deactivation take place simultaneously. The resulting set of partial differential equations has been solved by a program written in Matlab, using a numerical procedure based on finite differences.

The kinetic parameters of best fit and their confidence intervals have been determined by multivariable non-linear regression, using the Levenberg–Marquardt algorithm. The objective function, Φ , is the sum of square residuals corresponding to the differences between the experimental values and those calculated for the composition of the different lumps of the kinetic scheme. The kinetic constants have been reparameterized [15] in order to reduce the correlation between the estimations of frequency factor and activation energy. Consequently, the parameters calculated are the kinetic constants for a reference temperature (350 °C) and the corresponding activation energies.

Different alternatives have been studied for Eq. (6) and for Eqs. (4) and (7), by setting different values of the parameters d , n and n_d . The discrimination of the kinetic models has been carried out on the basis of the statistics calculated for the Fischer distribution.

Table 1

Kinetic constants, deactivation order and functions for attenuation by water, corresponding to the model of best fit

Kinetic constant (h^{-1})	k_i (at 350 °C) (h^{-1})	E (kcal mol^{-1})	Deactivation order and functions for attenuation by water
k_O	7.023 (± 0.297)	13.66 (± 0.391)	$d = 1.5$
k_{CH_4}	5.62×10^{-3} ($\pm 4.29 \times 10^{-3}$)	30.34 (± 6.234)	$\theta = \frac{1}{1+K_W X_W}$
k_2	2.39×10^{-3} ($\pm 2.04 \times 10^{-3}$)	16.60 (± 12.22)	$\theta_d = \frac{1}{1+(X_W)^{1.5}}$
k_3	171.6 (± 6.035)	13.23 (± 0.682)	
k_d	31.36 (± 18.36)	6.299 (± 5.13)	
K_W	0.634 (± 0.025)		

3.3. Fit of the kinetic model to the experimental results

Table 1 shows the kinetic parameters calculated for the kinetic model of best fit and their corresponding intervals for 90% confidence. The value of the objective function corresponding to the optimum is $\Phi = 1.263$ and the variance corresponding to the optimum $\sigma_f^2 = 1.083 \times 10^{-3}$. The fit of the experimental results of olefin and methane concentration with time on stream at the reactor outlet to the kinetic model is shown in Fig. 2, for some of the experimental conditions studied. The suitability of the fit between the experimental (points) and the results calculated with the kinetic model by using the calculated kinetic parameters

(lines) is evidence of the validity of the model for the MTO process on SAPO-18.

The kinetic model proposed allows for ascertaining magnitudes of interest that are either theoretical or applicable to the reactor design. Fig. 3 shows the evolution with time on stream of three characteristic properties of the MTO process for different temperatures and water contents in the feed. These properties calculated by solving the kinetic model are: catalyst activity; the parameter that quantifies the standardised amount of intermediate compounds trapped in the cages of SAPO-18, $\alpha = Y/(Y_R)_{\text{max}}$, and olefin production rate, r_O . It is observed that, as temperature is increased (right graphs), catalyst activity decreases more

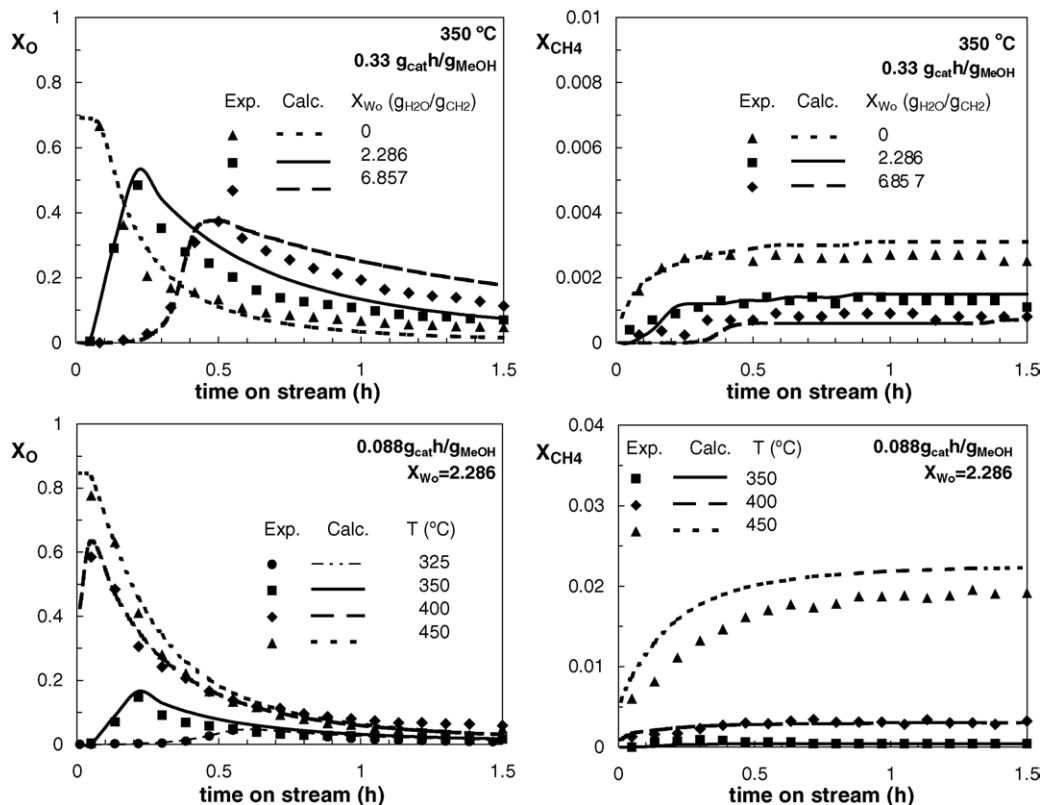


Fig. 2. Evolution with time on stream of experimental (points) and calculated (lines) values of mass fraction (by CH_2 mass unit) of olefins (left) and methane (right). Upper graphs: different water content in the feed, at 350 °C and $0.33 (\text{g catalyst}) \text{ h} / (\text{g MeOH})^{-1}$. Lower graphs: different temperatures for $0.088 (\text{g catalyst}) \text{ h} / (\text{g MeOH})^{-1}$ and 50 wt% water in the feed.

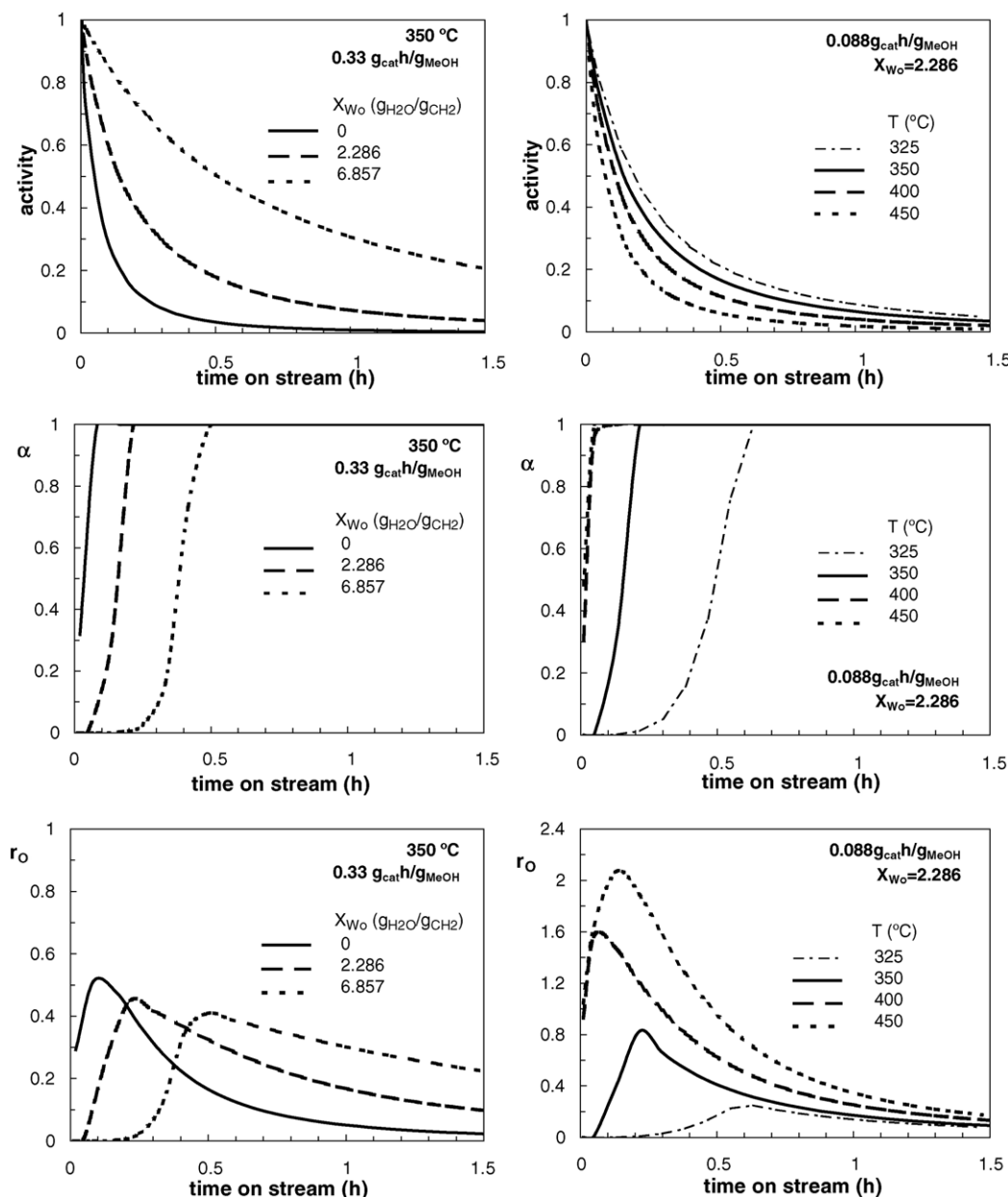


Fig. 3. Effect of water content in the feed (left) and temperature (right) on the evolution with time on stream of catalyst activity, amount of intermediate compounds and olefin production rate.

rapidly, but the formation of the intermediate compound is much faster, and above $400\text{ }^{\circ}\text{C}$ the maximum concentration of the intermediate compound is reached almost at the beginning of the reaction. Reaction rate peaks for olefin formation are also observed and these are reached at a lower time on stream as temperature is increased. The increase of water content in the feed (left graphs in Fig. 3) contributes to attenuating the deactivation rate and delays the period of reactive intermediate growth when reaction temperature is low ($350\text{ }^{\circ}\text{C}$), although this latter effect is notably attenuated at higher temperatures. The maximum reaction rate for olefin formation is reached for the time on stream for which the concentration of reactive intermediates is maximum.

4. Conclusions

The kinetic model proposed for the MTO process on SAPO-18 takes into account the evolution with time on stream of the concentration of the oxygenate lump, olefins and methane, in a wide range of operating conditions. Consequently, it is a useful tool for the design of the reactor and for estimating the interest of SAPO-18 as an alternative to the SAPO-34 presently used in industry.

Although the kinetic model is simplified because it provides the concentration of oxygenate and olefin lumps, it takes into account recent theories on the mechanistic aspects of the transformation of methanol into olefins, such as the

formation of active intermediate compounds that are trapped in the cages of the catalyst. This way, the initiation step is quantified, which is important in a wide range of experimental conditions, due to the need for feeding water for attenuating coke deposition. The kinetic model contemplates the deactivation from zero time on stream as a process of inactivation of active intermediates and, consequently, the rate of olefin formation peaks at a time on stream corresponding to the maximum concentration of active intermediates in the catalyst. Moreover, the treatment given in this paper to deactivation by assuming that it occurs in parallel with the initiation step is applicable to other catalytic processes that also require an initiation step for activating the formation of products.

Acknowledgements

This work has been carried out with the financial support of the University of the Basque Country (Project 9/UPV 00069.310-13607/2001), the Ministry of Science and Technology of the Spanish Government (Project PPQ2003-5645) and a researchers training grant (BFI03.313) from the Basque Government.

References

- [1] J.R. Rostrup-Nielsen, *Catal. Today* 712 (2002) 243.
- [2] T.-Y. Park, G.F. Froment, *Ind. Eng. Chem. Res.* 40 (2001) 4172.
- [3] T.-Y. Park, G.F. Froment, *Ind. Eng. Chem. Res.* 40 (2001) 4187.
- [4] S.M. Alwahabi, G.F. Froment, *Ind. Eng. Chem. Res.* 43 (2004) 5098.
- [5] G. Pop, G. Musca, D. Ivanescu, E. Pop, G. Mari, E. Chirila, O. Muntean, in: L.F. Albright, B.L. Crynes, S. Nowak (Eds.), *Novel Production Methods for Ethylene, Light Hydrocarbons, and Aromatics*, Marcel Dekker Inc., New York, 1992, p. 443.
- [6] A.N.R. Bos, P.J. Tromp, H.N. Akse, *Ind. Eng. Chem. Res.* 34 (1995) 3808.
- [7] A.G. Gayubo, A.T. Aguayo, A.E. Sánchez del Campo, A.M. Tarrío, J. Bilbao, *Ind. Eng. Chem. Res.* 39 (2000) 292.
- [8] A.G. Gayubo, A.T. Aguayo, A.E. Sánchez del Campo, P.L. Benito, J. Bilbao, *Stud. Surf. Sci. Catal.* 126 (1999) 129.
- [9] J. Chen, J.M. Thomas, P.A. Wright, R.P. Townsend, *Catal. Lett.* 28 (1994) 241.
- [10] A.T. Aguayo, A.G. Gayubo, R. Vivanco, M. Olazar, J. Bilbao, *Appl. Catal. A: Gen.* 283 (2005) 197.
- [11] I.M. Dahl, S. Kolboe, *J. Catal.* 149 (1994) 458.
- [12] W. Song, J.F. Haw, J.B. Nicholas, C.S. Heneghan, *J. Am. Chem. Soc.* 122 (2000) 10726.
- [13] A.G. Gayubo, R. Vivanco, A. Alonso, B. Valle, A.T. Aguayo, *Ind. Eng. Chem. Res.* (2005), in press.
- [14] A.G. Gayubo, A.T. Aguayo, A.L. Morán, M. Olazar, J. Bilbao, *AIChE J.* 48 (2002) 1561.
- [15] A.K. Agarwal, M.L. Brisk, *Ind. Eng. Chem. Process Des. Dev.* 24 (1985) 203.